On the Relationship Between the Brewer-Dobson Circulation and the Southern Annular Mode During Austral Summer in Coupled Chemistry-Climate Model Simulations

Feng Li[1], Paul A. Newman[2], and Richard S. Stolarski[2]

[1]Goddard Earth Sciences and Technology Center, University of Maryland, Baltimore County, Baltimore, Maryland, USA
[2]Atmospheric Chemistry and Dynamics Branch, NASA Goddard Space Flight Center, Greenbelt, Maryland, USA

Popular Summary

The Brewer-Dobson circulation (BDC) is the mean transport circulation in the stratosphere. It consists of an upwelling branch in the tropics, poleward flows from the tropics to the extratropics, and downward flows in the extratropics. The BDC plays a crucial role in the distribution of important stratospheric trace gases, such as ozone and water vapor. Therefore changes in the strength of the BDC under global warming could have significant impact on stratospheric ozone depletion and recovery. For example, all climate models that are used by the World Meteorological Organization to predict ozone evolution in the 21st century project a strengthening of the BDC that leads to ozone super-recovery in the mid-latitudes. On the other hand, ozone changes could also affect the strength of the BDC.

This work investigates an outstanding question: whether and how changes in the Brewer-Dobson circulation are connected to climate change in the troposphere, in particular, the annular modes. The annular modes are the leading variability in the extratropical troposphere, which describes a seesaw pattern of circulation fluctuations between the polar and middle latitudes. Using simulations from the Goddard Earth Observing System Coupled Chemistry Climate Model (GEOS CCM), we found the strengthening of the BDC in the summer Southern Hemisphere is strongly correlated with a shift of the Southern Hemisphere Annular Mode (SAM) toward its positive phase for the last 4 decades of the 20th century. This relationship is only present in model runs that simulate the stratospheric ozone depletion. Therefore it is concluded that the BDC-SAM relationship is driven by Antarctic ozone depletion. The ozone hole significantly cools the Antarctic stratosphere in late spring/early summer, which leads to a delayed breakdown of the polar vortex: strong circumpolar eastward flows that usually shift to westward winds in late spring. The prolonged persistence of stratospheric eastward flow enhances upward propagation of tropospheric waves into the stratosphere and strengthens the BDC. The increased wave flux in the stratosphere in turn drives a SAM trend toward its positive phase. Our results also show that the BDC-SAM relationship is robust on the interannual timescale.

Relationships between the Brewer-Dobson circulation and the southern annular mode during austral summer in coupled chemistry-climate model simulations

Feng Li[1], Paul A. Newman[2], and Richard S. Stolarski[2]

[1] Goddard Earth Sciences and Technology Center, University of Maryland Baltimore County, Baltimore, USA

[2] NASA Goddard Space Flight Center, Greenbelt, USA

Correspondence to: Feng Li (feng.li@nasa.gov)

Abstract

The Brewer-Dobson circulation (BDC) is the mean meridional mass circulation in the stratosphere and the Southern Annular Mode (SAM) is the prime variability pattern of the Southern Hemisphere extratropical troposphere. Motivated by previous studies showing that both the strength of the BDC and the SAM have the largest trends in the austral summer in the recent past, this paper investigates the relationships between the BDC and the SAM using coupled chemistry-climate model simulations. The model results show that the strengthening of the BDC in the Southern Hemisphere during November-February (NDJF) is strongly projected onto the high index of the SAM. The BDC-SAM relationship is driven by Antarctic ozone depletion, which increases stratosphere-troposphere interactions through a delayed Antarctic vortex breakup. The prolonged persistence of stratospheric westerlies enhances upward propagation of tropospheric wave activity into the stratosphere and strengthens the BDC. The wave flux and westerly anomalies in the stratosphere in turn drives a SAM trend toward its high index. Model results also show that the BDC-SAM relationship is robust on the interannual timescale.

1 Introduction

The stratospheric mean meridional circulation, or the so-called Brewer-Dobson circulation (BDC), plays a crucial role in the distribution of ozone and other important trace species in the stratosphere [*Brewer* 1949; *Dobson* 1956]. The BDC consists of an upwelling branch in the tropics, poleward flows, and downwelling branches in the extratropics [*Andrews et al.*, 1987]. The forcing of the BDC is from Rossby and gravity wave breaking in the extratropical stratosphere, which deposits westward momentum in the atmosphere that drives a poleward flow [*Holton et al.*, 1995]. Because of mass continuity, poleward flow in the extratropical stratosphere induces rising motion in the tropics and sinking motion in the mid-to-high latitudes.

Butchart and Scaife [2001] were the first to predict a strengthening of the BDC in response to greenhouse gas (GHG) increase. Because an enhanced BDC has significant impacts on stratospheric transport, ozone recovery, and stratosphere-troposphere exchange, the strength of the BDC under global warming has been extensively investigated. Numerous middle-atmosphere model simulations have confirmed that an increase in the BDC is a robust model response to climate change [e.g., *Butchart et al.,* 2006]. Model results indicate that the acceleration of the BDC is caused by a stronger stratospheric wave forcing with contributions from both model resolved waves and parameterized gravity waves [*Butchart et al.*, 2006; *Li et al.*, 2008; *Garcia and Randel*, 2008; *McLandress and Shepherd*, 2009]. Several studies have linked the increase in the stratospheric wave driving to GHG increase, sea surface temperature change, and

51 stratospheric ozone depletion [*Butchart and Scaife*, 2001; *Li et al.*, 2008; *Garcia and*
52 *Randel*, 2008; *Omen et al.*, 2009].
53
54 Despite extensive studies of the BDC, there are still some outstanding dynamical
55 questions. One important issue is whether and how changes in the BDC are connected to
56 climate change in the troposphere, in particular, the annular modes. The annular modes
57 are the leading variability in the extratropical troposphere at intraseasonal, interannual,
58 and decadal timescales [*Thompson and Wallace*, 2000; *Thompson et al.*, 2000]. When
59 the zonal-mean zonal wind in the stratosphere is weak westerly, the annular modes are
60 coupled with the stratospheric circulation through active wave – mean flow interactions.
61 During these active seasons, wind variability associated with the annular modes can
62 modulate Rossby wave propagation into and within the stratosphere, and hence can
63 modulate the strength of the BDC. On the other hand, increased wave – mean flow
64 interactions in the stratosphere can affect tropospheric variability reflected as changes in
65 the annular modes [*Hartmann et al.,* 2000]. Previous work on the relationship between
66 the annular modes and the BDC has focused on their interannual variations. For
67 example, *Limpasuvan and Hartmann* [2000] and *Hartmann et al.* [2000] found that a
68 high index of the Northern Annular Mode (NAM) is associated with a poleward shift of
69 the tropospheric jet and a stronger polar vortex, which decreases the refractive index and
70 leads to a reduction of the stratospheric wave drag and a weaker BDC. But this
71 relationship appears to hold only on the interannual timescale [*Hu and Tung*, 2002]. In
72 the Southern Hemisphere (SH), *Fogt et al.* [2009] found that the spring stratospheric
73 wave driving is significantly correlated with the summer Southern Annular Mode (SAM),

74 suggesting a close relationship between the BDC and SAM on the intra- and inter- annual
75 timescale.
76
77 At present, the relationship between the annular modes and the strength of the BDC over
78 the decadal timescale is poorly understood. The motivation of this paper is the similar
79 seasonality of the trends in the SAM and the BDC in the late 20th century, which suggests
80 that the long-term trends in the SAM and the BDC could be closely related. The SAM is
81 the dominant pattern of variability in the SH troposphere, which describes the
82 fluctuations in geopotential height, temperature, zonal wind, and surface pressure with
83 opposite signs in high and middle southern latitudes [*Thompson and Wallace*, 2000].
84 Observational studies have identified a significant trend of the SAM toward its positive
85 phase (or a high index) during the late 20th century, characterized by a strengthening of
86 the Antarctic polar vortex and a poleward shift of the tropospheric jet with the largest
87 seasonal trend occurring in the austral summer [*Thompson and Solomon*, 2002; *Marshall*,
88 2003]. Similar seasonality in the trend of the BDC has been reported in a number of
89 coupled chemistry-climate model (CCM) investigations [*Butchart et al.*, 2006; *Li et al.*,
90 2008]. *Li et al.* [2008] further showed that this seasonal structure in the BDC trend is
91 mainly caused by large increases in the SH downwelling during the austral summer. In
92 addition, previous studies have found that Antarctic ozone depletion has a significant
93 impact on the seasonality of the trends in the SAM [*Cai and Cowen*, 2007; *Perlwitz et al.*,
94 2008] and the BDC [*Li et al.*, 2008; *McLandress and Shepherd*, 2009; *Oman et al.*,
95 2009].
96

97 The purpose of this paper is to investigate whether and how trends in the SAM and the
98 BDC are related in the austral summer by examining simulations from the Goddard Earth
99 Observing System (GEOS) CCM. We focus on the BDC-SAM relationship over the
100 decadal timescale, but we also address their link on the interannual timescale. The model
101 and simulations used in this paper are described in the next section. Results are presented
102 in Section 3. Conclusions and discussions are given in Section 4.
103

104 ## 2 Model and Simulations

105
106 This study uses simulations with version 1 of the GEOSCCM. Details of the model can
107 be found in *Pawson et al.* [2008]. The model is an extension of the GEOS-4 General
108 Circulation Model with a comprehensive stratospheric chemistry module. It uses a flux-
109 form semi-Lagrangian dynamical core and the physics are adapted from the NCAR
110 CCM3. The stratospheric chemistry module is from the Goddard Chemical Transport
111 Model [*Douglass et al.*, 1996]. The model chemistry is coupled with the physical
112 processes through the radiation code. The model has 55 vertical levels with a top at 0.01
113 hPa. Simulations used in this study were performed with a horizontal resolution of 2^{o}
114 latitude by 2.5^{o} longitude.
115
116 For this study, we present results from three simulations of the latter half of the 20^{th}
117 century (1960-2000). The first two experiments P1 and P2 are a two-member ensemble
118 simulation (with different initial conditions) forced with observed, time-dependent sea
119 surface temperature and sea ice amounts from HadISST, and the CCMVal REF1 scenario
120 of GHGs and ozone-depleting substances (ODSs) [*Eyring et al.*, 2005]. The mean of P1

and P2 in this study is denoted as P12. The third run Cl60 is identical to the first two except that the halogen concentrations are fixed at 1960 levels. The purpose of Cl60 is to separate the impacts of GHG and ODS.

Eyring et al. [2006] evaluated simulations of temperature, trace species, and ozone for the period 1980-1999 from P1 and twelve other CCMs. *Pawson et al.* [2008] assessed ozone-temperature coupling in P1 and P2. Overall P1 and P2 results agree well with observations in terms of the stratospheric thermal structure and trace gas distributions. Long-term stratospheric temperature trend and ozone depletion in P1 and P2 are in reasonable agreement with observations. As with other CCMs, GEOSCCM has biases. One that is relevant to this study is that the Antarctic vortex is too persistent [*Pawson et al.*, 2008; *Hurwitz et al.*, 2009]. This will be discussed in Section 4.

3 Model Results

A key factor to understand the relationship between the trends in the BDC and SAM is their seasonality. This is illustrated by comparing the seasonal structure of trends in the net SH downward mass flux and the Antarctic geopotential height in the P12 simulations, which represent the seasonality of trends in the BDC and the SAM, respectively (Fig. 1). Here and for the rest of this study, the trend is calculated by a linear least-squares regression. The statistic significance of the trend is calculated using a two-tailed Student's t-test with the degrees of freedom reduced from a lag-1 autocorrelation of

143 regression residuals [*Santer et al.,* 2000]. The net hemispheric downward mass flux has
144 been widely used as a measure of the strength of the BDC and is calculated by

145 $$2\pi \int_{\varphi_t}^{pole} a\rho \cos\varphi \overline{w^*} d\varphi$$

146 where $\overline{w^*}$ is the residual vertical velocity, ρ is the density, a is the Earth's radius, and φ_t
147 is the southern turnaround latitude where the tropical upwelling changes to extratropical
148 downwelling [*Butchart et al.*, 2006]. The SAM characterizes the seesaw pattern of
149 geopotential height changes between Antarctica and the middle latitudes, and thus the
150 seasonal structure of the trend in the Antarctic geopotential height can illustrate the
151 seasonality of the trend in the SAM [*Thompson and Solomon*, 2002]. Figure 1 shows that
152 the net SH downward mass flux at 30 hPa (1a) and the Antarctic geopotential height at
153 850 hPa (1b) have the largest and statistically significant (95% confidence level) trends in
154 the austral late spring and summer (November - February). The increase in the net SH
155 downwelling indicates an acceleration of the southern BDC, whereas the falling of the
156 geopotential height indicates a trend of the SAM toward its positive phase. If we
157 calculate the trends for the seasonal mean net downward mass flux, then both the summer
158 (December-February) and winter (June-August) trends are statistically significant, but the
159 summer trend is about 1/3 larger than the winter trend. Similar seasonal structure in the
160 net SH downward mass flux is found in other lower stratosphere levels. For the
161 geopotential height change over the Antarctic troposphere, Figure 1b shows smaller but
162 statistically significant decreasing trend in April. This seasonal structure in the P12
163 simulations agrees well with *Thompson and Solomon* [2002] who identified substantial
164 decreasing trend in the tropospheric geopotential height over Antarctic in the austral
165 summer and fall using radiosonde data.

166

167 Figure 2a shows the seasonal evolution of the Antarctic geopotential height trend for the
168 period 1960-2000. In the stratosphere, the geopotential height within the polar cap
169 decreases from October to May with the largest drop in late spring and early summer
170 (statistically significant at the 95% confidence level). This large decrease in the
171 stratospheric geopotential height from November to February is caused by a strong
172 cooling in the Antarctic lower stratosphere that peaks in November and extends to
173 February (Fig. 2b, recall that, assuming constant surface pressure, geopotential height
174 represents the vertical integral of temperature $Z(p) = -\int_{psurf}^{p} \frac{RT(p)}{g} d\ln p$). During
175 November-January, the geopotential height decrease extends from the stratosphere to the
176 surface (Fig. 2a). These features agree very well with observations [*Thompson and*
177 *Solomon*, 2002]. The cooling in the Antarctic lower stratosphere also produces a large
178 westerly shift of the circumpolar flow in the stratosphere that is coupled with an
179 enhanced westerly flow throughout the troposphere from November to January (Fig. 2c).
180

181 Several observational [*Thompson and Solomon*, 2002] and modeling studies [*Cai and*
182 *Cowen*, 2007; *Perlwitz et al.*, 2008] have suggested that the large summer SAM trend is
183 related to Antarctic ozone depletion. Strengthening of the BDC during the austral
184 summer in the recent past has also been largely attributed to Antarctic ozone depletion
185 [*Manzini et al.*, 2003; *Li et al.*, 2008; *McLandress and Shepherd*, 2008]. In our
186 simulations the role of Antarctic ozone depletion in driving trends in the BDC and the
187 SAM can be clarified by comparing the P12 and Cl60 results. Again, Cl60 is same as
188 P12 except that the halogen loading is fixed at 1960 levels, and therefore has no Antarctic

189 ozone hole. Without ozone depletion there is no significant trend in the 30 hPa net SH
190 downward mass flux in December-February (Figure 3a) when the P12 simulations show
191 the largest increase (see Fig. 1a for comparison). The trend in the Antarctic geopotential
192 height at 850 hPa in Cl60 (Fig. 3b) also has totally different seasonal structures from that
193 in P12 (see Fig. 1b). The lower tropospheric geopotential height over Antarctica actually
194 increases (although not statistically significant) in late spring and early summer in Cl60
195 (also see Fig. 4a), due to GHG-increase induced tropospheric warming (Fig. 4b).
196 Comparing temperature changes in the Antarctic stratosphere between Cl60 and P12
197 reveals that the strong lower stratosphere cooling and the significant middle stratosphere
198 warming is driven by the ozone hole (Figs. 4b and 2b). Figure 4c shows that in Cl60 the
199 circumpolar flow does not have a significant trend from November to February in the
200 troposphere and stratosphere, in contrast to the strong westerly accelerations in the P12
201 simulations. These different changes between the P12 and Cl60 simulations clearly show
202 that the large summer SAM and BDC trends are driven by Antarctic ozone depletion.
203
204 The connection between Antarctic ozone depletion and the strengthening of the BDC in
205 the SH is well understood [e.g., *Li et al.,* 2008]. Ozone hole cools the Antarctic lower
206 stratosphere, increases the meridional temperature gradient in the sub-polar region, and
207 strengthens the westerly circumpolar flow. As a result, the breakup of the Antarctic polar
208 vortex is delayed from late spring to early summer. A direct consequence of the delayed
209 polar vortex breakup is that the stratospheric planetary wave activity emanating from the
210 troposphere can penetrate higher and stay longer in the stratosphere, causing an
211 acceleration of the BDC. It should be noted that an underlying assumption of the above

212 argument is that the strengthening of the southern BDC can be accounted for by increases
213 in the planetary wave forcing. Therefore we first need to verify whether this is indeed the
214 case in the P12 simulations in order to apply the delayed polar vortex breakup mechanism
215 to explain the seasonality of the BDC trend.
216
217 Figure 5 compares the evolution of the November-February (NDJF) 30 hPa net SH
218 downward mass flux and the contributions from model resolved waves and parameterized
219 gravity waves calculated from the downward control principle [*Haynes et al.*, 1991]. We
220 choose NDJF because the net SH stratospheric mass flux increase and the lower
221 tropospheric Antarctic geopotential height drop are largest during this four-month period
222 (see Fig. 1). Figure 5 shows that the actual net SH mass flux agrees very well with the
223 wave-driven mass flux from the downward control analysis. Model resolved waves and
224 parameterized gravity waves account for, respectively, 72% and 28% of the net SH
225 downward mass flux at 30 hPa, consistent with previous studies [e.g., *Butchart et al.*,
226 2006]. The long-term and interannual variations of the mass flux driven by EP-flux
227 divergence are in very good agreement with the actual mass flux with a correlation of
228 0.97. We conclude that the strengthening of the SH extratropical BDC is mostly due to
229 increase in the stratospheric planetary wave forcing.
230
231 Figure 5 also shows that the change of the net SH downwelling during NDJF is not a
232 linear trend. There is an abrupt change around 1980 and the trend for the period 1981-
233 2000 is much larger than that for the period 1960-1980. We found that the NDJF net SH
234 downwelling is highly correlated with the October Antarctic total ozone (r=0.90) (Fig. 6),

235 which suggests that the strength of the southern summer BDC is strongly affected by the
236 severity of Antarctic ozone depletion. Similar temporal structures are also found in the
237 evolution of the Antarctic geopotential height during NDJF in both the troposphere and
238 the stratosphere (Fig. 6). The time series of the 30 hPa and 850 hPa geopotential height
239 are highly correlated with each other (r=0.78), and they are both strongly correlated with
240 the October Antarctic total ozone (r=0.89 and 0.59, respectively) and the 30 hPa net SH
241 downward mass flux (r=0.78 and 0.62, respectively). *Thompson and Solomon* [2002]
242 identified strong correlations between Antarctic ozone depletion and the falling of the
243 tropospheric and stratospheric geopotential height in the southern high latitudes using
244 observational data and argued that these correlations suggest a significant impact of the
245 ozone hole on the SAM trend. Our P12 results support their argument and also reveal a
246 possible linkage between the BDC and SAM through their close connection with the
247 Antarctic ozone hole.
248
249 The relationship between the changes in the southern extratropical BDC and SAM in the
250 P12 simulations is investigated by comparing the trend of the residual circulation with the
251 regression (or covariance) of the residual circulation on the SAM index. We follow the
252 method of *Thompson et al.* [2000] to define the SAM as the first empirical orthogonal
253 function (EOF) of the 850 hPa geopotential height southward of 20°S. The EOFs are
254 calculated using NDJF mean time series for the period 1981-2000 and the standardized
255 leading principal component time series are used as the SAM index. The calculated
256 SAM index using this method is very similar to the inverted 850 hPa Antarctic
257 geopotential height (see Fig. 6). Results presented in the following are not sensitive to

258 the definition of the SAM pattern and index. For example, we can use the circumpolar
259 upper tropospheric zonal wind as the SAM index and obtain the same results. We focus
260 on the 20-year period 1981-2000 because changes in the BDC and SAM are much larger
261 than those in the period 1960-1980 (Fig. 6).
262
263 The linear trend of the residual vertical velocity in NDJF between 1981 and 2000 in P12
264 is shown in Fig. 7a as a function of latitude and pressure. In the stratosphere, trend in the
265 residual vertical velocity demonstrates an accelerated BDC with enhanced downwelling
266 in the southern high latitudes (dashed contours) and increased upwelling in the mid-
267 latitudes (solid contours). Very similar spatial patterns are found in the SAM regression
268 map (Fig. 7b), showing that an anomalously strong BDC is associated with a high index
269 of the SAM. The nearly identical patterns in Figs. 7a-b illustrate that the long-term
270 change of the strengthening of the BDC is highly projected onto the trend of SAM toward
271 its high index. The trend in the residual vertical velocity that is linearly congruent with
272 the SAM index, obtained by multiplying the covariance with the linear trend of the SAM
273 index, can be used to quantify the relationship between trends in BDC and SAM
274 [*Thompson and Solomon*, 2002]. The SAM index has a linear trend of 0.90/decade for
275 the period 1981-2000 in the P12 simulations, thus it can be inferred that more than 80%
276 of increases in the Antarctic downwelling and mid-latitude upwelling are linearly
277 congruent to the SAM index. Furthermore, almost all the tropospheric trend in the
278 residual vertical velocity is linearly projected onto the SAM.
279

280 Although the BDC does not show a significant linear trend in NDJF in Cl60 (Fig. 3a), it
281 is still worthy to examine whether the interannual variations of the BDC are related to
282 those of SAM in Cl60. Figure 8a shows that the linear trend in the stratospheric residual
283 vertical velocity is not statistically significant and does not resemble the SAM regression
284 map. However, the SAM index regression map in Cl60 (Fig. 8b) has a nearly identical
285 pattern to that for P12 (Fig. 7b). The magnitude of the regression coefficients is smaller
286 in Cl60 than in P12, because the trends of the BDC and SAM in P12 yield larger
287 covariance. When the covariance between the residual vertical velocity and the SAM in
288 P12 is calculated using detrended data, the resulting regression coefficients have nearly
289 the same magnitude as those in Cl60 (figure not shown). The similar regression patterns
290 in P12 and Cl60 illustrate that, regardless of ozone depletion, a high SAM index is
291 associated with anomalously strong polar downwelling and mid-latitude upwelling in
292 austral summer on the interannual timescale. Without ozone depletion, this relationship
293 only holds as year-to-year variability in Cl60. The impact of the Antarctic ozone hole is
294 to drive a long-term trend in the BDC that is strongly congruent with the year-to-year
295 SAM variations.
296
297 In order to understand why trends in the southern BDC are strongly reflected in the SAM
298 index in the P12 simulations, we need to find out the cause for the acceleration of the
299 BDC and its connection with the SAM. We have already shown in Fig. 5 that the
300 strengthening of the BDC in the austral summer is mostly due to increase in the
301 stratospheric planetary wave driving. Thus the question is how the enhanced planetary
302 wave driving is related to the SAM. To answer this question, we examine the linear

303 trends in the NDJF zonal mean temperature, zonal wind, eddy momentum and heat flux
304 between 1981 and 2000 and their SAM regression maps (Fig. 9). Temperature changes
305 in the summer Antarctic stratosphere are marked by a vertical dipole structure (Fig. 9a)
306 that has been reported in many model simulations [e.g., *Mahlman et al.*, 1994] and has
307 been confirmed in radiosonde and reanalysis data [*Randel and Wu*, 1999]. The strong
308 Antarctic lower stratospheric cooling increases the meridional temperature gradient and
309 enhances the stratospheric westerlies over the high latitudes (Fig. 9b). In NDJF, a
310 westerly shift of the SH stratospheric flow indicates a delay of the polar vortex breakup,
311 which prolongs the period of weak westerlies in the lower stratosphere and increases the
312 upward propagation of planetary wave activity into the stratosphere. This is illustrated in
313 Fig. 9c showing a large increase in negative northward meridional eddy heat flux (an
314 approximation of the vertical component of the EP flux) in the stratosphere poleward of
315 about 50°S, which increases westward momentum deposition and strengthens the BDC.
316 The westerly accelerations of the zonal wind in the SH high latitude stratosphere is
317 coupled with increased westerlies in the troposphere centered at 60°S (Fig. 9b). The
318 tropospheric zonal wind trend is characterized by a dipole structure, indicating a
319 poleward shift of the tropospheric jet. This poleward shift is maintained by a similar
320 displacement of the eddy meridional flux of zonal momentum in the upper troposphere
321 (Fig. 9d).
322
323 The SAM regression maps of the temperature, zonal wind, and eddy heat and momentum
324 flux are presented in Figs. 9e-h. Nearly identical patterns are found between the
325 regression maps and the linear trends, indicating that trends in the tropospheric and

326 stratospheric circulations and wave activities are strongly projected onto the positive
327 phase of the SAM. Multiplying the regression maps with the linear trend in the SAM
328 index and comparing, we found that nearly all trends in the troposphere are congruent
329 with the SAM index. More important for the purpose of this study, most of the
330 stratospheric trends (about 80%) are congruent with the SAM index.
331
332 Figures 10a-d show that the in the Cl60 simulation that does not include ozone depletion,
333 linear trends of the NDJF zonal wind, and eddy momentum and heat flux are not
334 statistically significant. Although Cl60 simulates statistically significant temperature
335 changes due to GHG increase, it does not reproduce the strong Antarctic lower
336 stratosphere cooling and middle stratosphere warming. Comparing with the P12 results
337 (Figs. 9a-d) clearly demonstrates that the trends in the P12 simulations are driven by the
338 ozone hole. However, the SAM regression maps in Cl60 are very similar to those in P12,
339 but with smaller covariance (Figs. 10 e-h). When we remove the trends in the P12 results
340 and calculate the regression, we find that the regression coefficients have nearly the same
341 magnitude in P12 and Cl60. This similarity indicates that the relationship between
342 interannual variations of the summer stratospheric circulation and SAM are robust, with
343 or without ozone depletion.
344
345 Our model simulated austral summer circulation changes and the SAM regression maps
346 are in broad agreement with those calculated using the National Centers for
347 Environmental Prediction (NCEP) Reanalysis 2 data. Figure 11 shows that the major
348 features of the SH summer climate change agree qualitatively very well between the

NCEP Reanalysis and the P12 runs, including the Antarctic lower stratospheric cooling, the strengthened circumpolar flow, and the enhanced stratospheric wave flux. There are no direct observations of the BDC (or the residual vertical velocity), but the increases of eddy heat flux in the mid-high latitude stratosphere in the NCEP Reanalysis (Fig. 11c) support the modeled strengthening of the BDC. Figure 11 also shows that the trends resemble the regressions onto the SAM index, supportive of the BDC-SAM relationship in our model simulations. However, GEOSCCM over-predicts the trends and the covariances with the SAM index. In the next section, we discuss why the BDC-SAM relationship is amplified in the simulations.

The above analyses suggest that the key to understand the BDC-SAM relationship in the austral summer is to link the circumpolar westerly anomalies and enhanced wave activity in the stratosphere to a high index of the tropospheric SAM. There is growing observational evidence that such stratospheric anomalies induce tropospheric variability reflected as a positive phase of the annular modes [e.g., *Baldwin et al.*, 2003; *Thompson et al.*, 2005; *Fogt et al.*, 2009]. Therefore a possible mechanism to explain the link between the ozone hole, the strengthening of the BDC, and the SAM trend is this: the ozone hole increases the stratospheric wave driving and strengthens the BDC through a delayed vortex breakup, which in turn forces a SAM trend toward its high index. One way to test this hypothesis is to remove the SAM variability that is linear congruent with the stratospheric wave driving, and check the relationship between the SAM residual and the ozone hole. If the SAM residual is correlated with the ozone hole and has a significant trend, this would suggest that other processes in addition to stratospheric wave

372 driving are involved in linking the ozone hole with the tropospheric SAM trend. We
373 found that after removing the part of SAM index that is congruent with the NDJF 30 hPa
374 mass flux, the SAM index residual does not have a statistically significant trend and is
375 not significantly correlated with the October total column ozone (r = -0.14 after removal
376 of trends) for the 1960-2000 period in the P12 runs (similar results are obtained for the
377 period 1981-2000 with r = -0.20). In comparison, as can be inferred from Figure 6, the
378 NDJF SAM index is highly correlated with October total ozone (r = -0.52 after removal
379 of trends) and has a statistically significant trend. These results appear to support our
380 hypothesis that Antarctic ozone depletion forces a summer tropospheric SAM trend
381 almost entirely through changes in stratospheric wave driving.
382

383 ## 4 Discussion and Conclusions

384

385 The relationship between the BDC and the SAM in the austral summer is investigated
386 with GEOSCCM simulations. In P12 that simulates ozone depletion, the southern BDC
387 accelerates and the SAM has a trend toward its positive phase during NDJF in the latter
388 half of the 20th century, and the strengthening of the BDC is strongly projected onto the
389 high index of the SAM. In contrast, in Cl60 that does not simulate ozone depletion,
390 neither the SAM nor the BDC has a significant trend during NDJF. These model results
391 clearly demonstrate that Antarctic ozone depletion drives the BDC-SAM relationship on
392 the decadal timescale. We suggest that the ozone-hole induced delay of the Antarctic
393 vortex breakup is the key to link the strengthening of the BDC with the SAM during the
394 austral summer. The delayed onset of easterlies in the Antarctic lower stratosphere

395 prolongs the period for dynamical stratosphere-troposphere interactions. A direct
396 consequence of the persistent stratospheric westerlies is to strengthen the summer BDC
397 by allowing more tropospheric planetary wave activity entering the stratosphere, as
398 shown in Figs. 9 and11. On the other hand, the enhanced stratospheric wave driving
399 forces a SAM trend toward its high index. In summary, the BDC-SAM relationship is a
400 result of increased stratosphere-troposphere coupling driven by ozone depletion.

401

402 Although the Cl60 simulation does not produce statistically significant trends in the BDC
403 and the SAM during NDJF, it reproduces the same interannual relationship between the
404 BDC and the SAM as that in the P12 simulations. And now the question is what drives
405 the year-to-year variability of the summer SAM and BDC. *Fogt et al.* [2009]
406 investigated intra-annual relationships between the Antarctic total column ozone, the
407 SAM, and the stratospheric wave activity in the latter half of the 20^{th} century using
408 observations and the same GEOSCCM simulations analyzed in this study. They found
409 that, in addition to the well-known negative correlation between the spring Antarctic
410 ozone and the summer SAM, the spring stratospheric wave driving also plays an
411 important role in determining the interannual variability of the summer SAM. The results
412 of *Fogt et al.* [2009] suggest, based on the positive correlation between the summer SAM
413 and BDC identified in this study, that the stratospheric wave activity (or BDC) in spring
414 could significantly affect the wave activity in summer, and is important in driving the
415 interannual BDC-SAM relationship. This is confirmed by the high negative correlation
416 between the early spring BDC and the summer SAM ($r = -0.56$ between October 30 hPa
417 SH mass flux and the NDJF SAM index), and between the early spring BDC and late

418 spring/early summer BDC (r = -0.55 between October and December/January 30 hPa mss
419 flux) in the P12 simulations (correlation is calculated after removal of linear trends).

420

421 We suggest that the mechanism by which the spring stratospheric wave activity affects
422 the interannual variability of the summer BDC and SAM is the same as that explaining
423 how ozone depletion drives the decadal variations of the summer BDC and SAM, i.e.,
424 through its impact on the persistence of the Antarctic vortex leading to changes in
425 stratosphere-troposphere coupling. *Hurwitz et al.* [2009] showed that the Antarctic polar
426 vortex breakup date is highly correlated with the spring stratospheric wave driving in the
427 NCEP and ERA40 reanalysis data and in the simulations with a newer version of
428 GEOSCCM. This relationship results from a 1-month lag correlation between the mid-
429 latitude wave driving and the polar stratospheric temperature [e.g., *Austin et al.,* 2003].
430 Anomalously weak eddy heat flux in early-middle spring leads to an anomalously cold
431 polar stratosphere in late spring and a delayed vortex breakup, which extends the period
432 of active stratosphere-troposphere dynamical coupling and causes a stronger summer
433 BDC and SAM. However, it should be emphasized that the decadal trends of the summer
434 BDC and SAM cannot be attributed to long-term changes in spring stratospheric wave
435 driving. In the P12 simulations the BDC in October does not have a statistically
436 significant trend (Fig. 1a). *Waugh et al.* [1999] found that in the NCEP reanalysis data
437 the SH eddy heat flux at 100 hPa in early spring increases from 1979 to 1998, which
438 cannot explain the prolonged persistence of the Antarctic vortex during this period.

439

440 It is interesting to compare the interannual BDC-SAM relationship identified in this paper
441 to the BDC-NAM relationship reported in previous studies. *Limpasuvan and Hartmann*
442 [2000] and *Hartmann et al.* [2000] found that a higher NAM index is associated with a
443 weaker stratospheric wave driving, and hence a weaker BDC, in the NH high latitudes
444 during the NH winter. This is opposite to the positive correlation between the BDC and
445 SAM during the austral summer. The different relationships between the BDC and the
446 annular modes in the NH and SH are due to the different seasonality of the SAM and
447 NAM. The NAM is actively coupled with the stratosphere circulation in winter, whereas
448 the SAM's active season is in late spring [*Thompson and Wallace*, 2000]. In the NH
449 winter a high NAM index is associated with a stronger Arctic vortex and stronger
450 circumpolar westerlies which decrease the refractive index and reduce wave activity
451 entering polar stratosphere [*Limpasuvan and Hartmann*, 2000; *Hu and Tung*, 2002]. But
452 in the SH summer a high SAM index is associated with a colder Antarctic lower
453 stratosphere, which delays the breakdown of the Antarctic vortex and strengthens the
454 BDC. From the above argument one expects that the BDC-SAM relationship would
455 reverse during the austral winter, and this is confirmed in the GEOSCCM simulations
456 (figure not shown).

457

458 There are no direct observations of the BDC, and hence the modeled BDC-SAM
459 relationship could not be directly verified. *Stolarski et al.* [2006] found indirect evidence
460 of a strengthened BDC from the observed ozone increase just above the ozone hole in the
461 austral summer in satellite measurements, which supports our findings. More
462 importantly, that the ozone-hole causes a delayed Antarctic vortex breakup leading to

463 increases in stratospheric wave flux, which is the key to understand the BDC-SAM
464 relationship, is reasonable represented in the model simulations compared with the NCEP
465 Reanalysis data. However, it is also apparent that the model over-predicts the BDC-SAM
466 relationship and the austral summer climate change.

467

468 As briefly mentioned in Section 2, GEOSCCM has a "cold pole" bias in the spring
469 Antarctic stratosphere, a common problem in middle atmosphere models [*Eyring et al.*,
470 2006]. Because of the cold bias, the modeled Antarctic vortex is too persistent and
471 breaks up about two weeks later than observed [*Hurwitz et al.*, 2009]. *Fogt et al.* [2009]
472 found that, as a consequence of the later than observed Antarctic vortex breakup,
473 GEOSCCM amplifies troposphere-stratosphere coupling and SAM persistence, and
474 hence over-predicts the spring ozone – summer SAM relationship. These model
475 deficiencies have important implications for the simulated BDC-SAM relationship
476 reported in this study, because this relationship is driven by stratosphere-troposphere
477 coupling. Therefore, while the simulated BDC-SAM relationship qualitatively agrees
478 with the reanalysis data, this relationship is amplified in our model simulations. More
479 generally, results presented here and those in *Fogt et al.* [2009] and *Hurwitz et al.* [2009]
480 indicate that a too persistent model Antarctic vortex leads to over-predictions of the
481 impacts of the ozone hole on the austral summer climate change in the late 20th century,
482 which also implies that the model would unrealistically amplify the ozone recovery
483 effects on climate change in the 21st century as well. Therefore, as pointed out by *Fogt et*
484 *al.* [2009] and *Hurwitz et al.* [2009], improving the model presentation of the persistence

485 of Antarctic vortex is critical to correctly predict the interactions between ozone
486 depletion, ozone recovery, and climate change in the troposphere and stratosphere.

487

488 Finally, the mechanism by which increased stratospheric wave activity drives a SAM
489 trend, or more generally the mechanism for the stratospheric variability to affect the
490 tropospheric circulation, is not clear. Currently there exist several hypotheses, including
491 downward propagation of wind anomalies driven by eddy-mean flow interactions
492 [*Christiansen*, 2001], amplification of tropospheric response to lower stratospheric wind
493 anomalies [*Song and Robinson*, 2004], and increases of tropospheric eddy phase speed
494 leading to a poleward displacement of the subtropical wave breaking zone [*Chen and*
495 *Held*, 2007]. There is growing evidence that the stratosphere has impacts on the
496 troposphere and understanding its dynamical mechanism is certainly an important
497 research issue.

498

499

500 **Acknowledgements**. This work was supported by NASA Modeling and Analysis
501 program. We thank three anonymous reviewers for their insightful comments. The
502 NCEP_Reanalysis 2 data are provided by the NOAA/OAR/ESRL PSD, Boulder,
503 Colorado, USA, from their Web site at http://www.esrl.noaa.gov/psd/.

504

505

505 **References**

506

507 Andrews, D. G., J. R. Holton, and C. B. Leovy [1987], *Middle Atmosphere Dynamics*,
508 485pp, Academic Press Inc., Orlando, Florida.

509

510 Austin, J., and co-authors [2003], Uncertainties and assessments of chemistry-climate
511 models of the stratosphere, *Atmos. Chem. Phys., 3*, 1-27.

512

513 Baldwin, M. P., D. B. Stephenson, D. W. J. Thompson, T. J. Dunkerton, A. J. Charlton,
514 and A. O'Neill [2003], *Science, 301*, 636-640.

515

516 Brewer, A. W. [1949], Evidence for a world circulation provided by the measurements of
517 helium and water vapor distribution in the stratosphere, *Q. J. R. Meterorol. Soc. 75*, 351-
518 363.

519

520 Butchart, N., and A. A. Scaife [2001], Removal of chlorofluorocarbons by increased
521 mass exchange between the stratosphere and troposphere in a changing climate, *Nature,*
522 *410*, 799-802.

523

524 Butchart, N., and coauthors [2006], Simulations of anthropogenic change in the strength
525 of the Brewer-Dobson circulation, *Clim. Dyn., 27*, 727-741.

526

527 Cai, W., and T. Cowan [2007], Trends in the Southern Hemisphere circulation in IPCC

528 AR4 models over 1950-99: ozone depletion versus greenhouse gas forcing, *J. Clim., 20*,
529 681-693.
530
531 Chen, G., and I. M. Held [2007], Phase speed spectra and the recent poleward shift of
532 Southern Hemisphere surface westerlies, *Geophys. Res. Lett., 24*, L21805,
533 doi:10.1029/2007GL031200.
534
535 Christiansen, B [2001], Downward propagation of zonal mean wind anomalies from the
536 stratosphere to the troposphere: Model and reanalysis, *J. Geophys. Res., 106*, 27,307-
537 27,322.
538
539 Dobson, G. M. B. [1956], Origin and distribution of the polyatomic molecules in the
540 atmosphere, Proc. R. Soc. London, Ser. A, 236, 187 – 193, doi:10.1098/rspa.1956.0127.
541
542 Douglass, A. R., C. J. Weaver, R. B. Rood, and L. Coy [1996], A three-dimensional
543 simulation of the ozone annual cycle using winds from a data assimilation system, *J.*
544 *Geophys. Res., 101*, 1463-1474.
545
546 Eyring, V., et al. [2005], A strategy for process-oriented validation of coupled chemistry-
547 climate models, *Bull. Am. Meteorol. Soc., 86*, 1117-1133.
548
549 Eyring, V., et al. [2006], Assessment of temperature, trace species, and ozone in
550 chemistry-climate model simulations of the recent past, *J. Geophys. Res., 111*, D22308,

551 doi:10.1029/2006JD007327.

552

553 Fogt, R. L., J. Perlwitz, S. Paswson, and M. A. Olsen [2009], Intra-annual relationships
554 between polar ozone and the SAM, Geophys. Res. Lett., 36, L04707,
555 doi:10.1029/2008GL036627.

556

557 Garcia, R. R., and W. J. Randel [2008], Acceleration of the Brewer-Dobson circulation
558 due to increases in greenhouse gases, *J. Atmos. Sci., 65*, 2731-2739..

559

560 Hartmann, D. L., J. M. Wallace, V. Limpasuvan, D. W. J. Thompson, and J. R. Holton
561 [2000], Can ozone depletion and global warming interact to produce rapid climate
562 change? *Proc. Natl. Acad. Sci., 92*, 1412-1417.

563

564 Haynes, P. H., C. J. Marks, M. E. McIntyre, T. G. Shepherd, and K. P. Shine [1991], On
565 the "downward control" of the extratropical diabitic circulation by eddy-induced mean
566 zonal forces, *J. Atmos. Sci., 48*, 651-678.

567

568 Hu Y., and K. K. Tung [2002], Interannual and decadal variations of planetary wave
569 activity, stratospheric cooling, and Northern Hemisphere annular model, *J. Clim., 15*
570 1659-1673.

571

572 Hurwitz, M. M., P. A. Newman, F. Li, L. D. Oman, O. Morgenstern, P. Braesicke, and J.
573 A. Pyle [2009], Assessment and consequences of the delayed breakup of the Antarctic

574 polar vortex in chemistry-climate models, *J. Geophsys. Res.*, in press.
575
576 Li, F., J. Austin, and J. Wilson [2008], The strength of the Brewer-Dobson circulation in
577 a changing climate: coupled chemistry-climate model simulations, *J. Clim., 21*, 40-57.
578
579 Limpasuvan V., and D. L. Hartmann [2000], Wave-maintained annular modes of climate
580 variability, *J. Clim., 13*, 4414-4429.
581
582 Mahlman, J. D., J. P. Pinto, and L. J. Umscheid [1994], Transport, radiative, and
583 dynamical effect of the Antarctic ozone hole: A GFDL "SKYHI" model experiment, *J.*
584 *Atmos. Sci., 51*, 489,508.
585
586 Manzini, E., S. C. Bruhl, M. A. Giorgetta, and K. Kurger [2003], A new interactive
587 chemistry-climate model: 2. Sensitivity of the middle atmosphere to ozone depletion and
588 increase in greenhouse gas and implications for recent stratospheric cooling, *J. Geophys.*
589 *Res., 108*, doi:10.1029/2002JD002977.
590
591 Marshall G. [2003], Trends in the southern annular modes from observations and
592 reanalyses, *J. Clim, 16*, 4134-4143.
593
594 McLandress, C., and T. Shepherd [2009], Simulated anthropogenic changes in the
595 Brewer-Dobson circulation, including its extension to high latitudes, *J. Clim*, *22*, 1516-
596 1540.

597

598 Oman, L., D. W. Waugh, S. Pawson, R. S. Stolarski, and P. A. Newman [2009], On the
599 influence of anthropogenic forcings on changes in the stratospheric mean age, *J.*
600 *Geophys. Res., 114*, D03105, doi:10.1029/2008JD010378.

601

602 Perlwitz, J., S. Pawson, R. L. Fogt, J. E. Nielsen, and W. D. Neff [2008], Impacts of
603 stratospheric ozone hole recovery on Antarctic climate, *Geophys. Res. Lett., 35*, L08714,
604 doi:10.1029/2008GL033317.

605

606 Pawson. S., R. S. Stolarski, A. R. Douglass, P. A. Newman, J. E. Nielsen, S. M. Frith,
607 and M. L. Gupta [2008], Goddard Earth Observing System chemistry-climate model
608 simulations of stratosphere ozone-temperature coupling between 1950 and 2005, *J.*
609 *Geophys. Res.,113*, D12103, doi:10.1029/2007JD009511.

610

611 Randel, W., and F. Wu [1999], Cooling of the Arctic and Antarctic polar stratosphere due
612 to ozone depletion, *J. Clim, 12*, 1467-1479.

613

614 Santer, B. D., T. M. L. Wigley, J. S. Boyle, D. J. Gaffen, J. J. Hnilo, D. Nychka, D. E.
615 Parker, and K. E. Taylor [2000], Statistical significance of trends and trend differences in
616 layer-average atmospheric temperature time series, *J. Geophys. Res.,105*, 7337-7356.

617

618 Stolarski, R. S., A .R. Douglass, M. Gupta, P. A. Newman, S. Pawson, M. R. Schoeberl,
619 and J. E. Nielsen [2006], An ozone increase in the Antarctic summer stratosphere: a

620 dynamical response to the ozone hole, *Geophys. Res. Lett., 33*, L21805,
621 doi:10.1029/2006GL026820.
622
623 Song, Y, and W. Robinson [2004], Dynamical mechanisms for stratospheric influence on
624 the troposphere, *J. Atmos. Sci., 61*, 1711-1725.
625
626 Thompson, D. W. J., and J. M. Wallace [2000], Annular Modes in the extratropical
627 circulation: Part I: month-to-month variability, *J. Clim, 13*, 1000-1016.
628
629 Thompson, D. W. J., J. M. Wallace, and G. C. Hegerl [2000], Annular Modes in the
630 extratropical circulation: Part II: trends, *J. Clim, 13*, 1018-1036.
631
632 Thompson, D. W. J., and S. Solomon [2002], Interpretation of recent Southern
633 Hemisphere climate change, *Science, 296*, 895-899.
634
635 Thompson, D. W. J., M. P. Baldwin, and S. Solomon [2005], Stratosphere-troposphere
636 coupling in the Southern Hemisphere, *J. Clim., 62*, 708-715.
637
638 Waugh, D. W., W. J. Randel, S. Pawson, P. A. Newman, and E. R. Nash [1999],
639 Persistence of the lower stratospheric vortices, *J. Geophy. Res., 104*, 27,191-27,201.
640

Figure Captions

Figure 1: Seasonal cycle of linear trends in the period 1960-2000 for (a) 30 hPa net SH downward mass flux, and (b) 850 hPa Antarctic (65°S-90°S) geopotential height in the P12 simulations. Shading indicates that trends are statistically significant at the 95% confidence level.

Figure 2: Linear trends plotted as function of month and pressure in (a) Antarctic geopotential height (65°S-90°S), (b) Antarctic temperature (65°S-90°S), and (c) circumpolar zonal wind (55°S-70°S) in the P12 simulations. Shading indicates that trends are statistically significant at the 95% confidence level.

Figure 3: Same as Fig. 1, but for the Cl60 simulation.

Figure 4: Same as Fig. 2, but for the Cl60 simulation.

Figure 5: Time series of the NDJF mean net SH downward mass flux at 30 hPa (black). The red and blue lines are the wave-driven mass fluxes calculated from the downward control principle. The red lines show the results from model resolved waves (EP-flux divergence) only. The blue lines show the results including both resolved waves and parameterized gravity waves. The thick curves are 7-year running average mean.

662 Figure 6: Time series of (upper panel) October Antarctic total ozone; (middle panel) the
663 negative of the NDJF mean net SH mass flux at 30 hPa; and (lower panel) NJDF mean
664 geopotential height at 30 hPa (green, left axis) and 850 hPa (blue, right axis). Thick
665 curves are 7-year running average mean.
666
667 Figure 7: (a) Linear trends of the NDJF residual vertical velocity in the period 1981-2000
668 as a function of latitude and pressure. Shading denotes that trends are significantly
669 different from zero at the 95% confidence level. (b) NDJF residual vertical velocity
670 regressed on the standardized SAM index.
671
672 Figure 8: Same as Fig. 7, but for the Cl60 simulation.
673
674 Figure 9: Upper panels show linear trends for the period 1981-2000 as a function of
675 latitude and pressure for the NDJF mean (a) temperature (K/decade), (b) zonal wind (ms^{-1}/decade),
676 (c) northward meridional eddy heat flux (Kms^{-1}/decade), and (d) meridional
677 eddy flux of zonal momentum (m^2s^{-2}/decade) in the P12 simulations. Shading denotes
678 the 95% confidence level. Lower panels are the SAM regression maps for the NDJF
679 mean (e) temperature (K/std SAM), (f) zonal wind (ms^{-1}/std SAM), (g) eddy heat flux
680 (Kms^{-1}/std SAM), and (h) eddy momentum flux (m^2s^{-2}/std SAM).
681
682 Figure 10: Same as Fig. 9, but for the Cl60 simulation.
683

684 Figure 11: Same as Fig. 9 but calculated from the NCEP Reanalysis 2 data. The dark and
685 light shadings denote 95% and 90% confidence levels, respectively. Note that the NCEP
686 data are only available below 10 hPa.
687
688

688

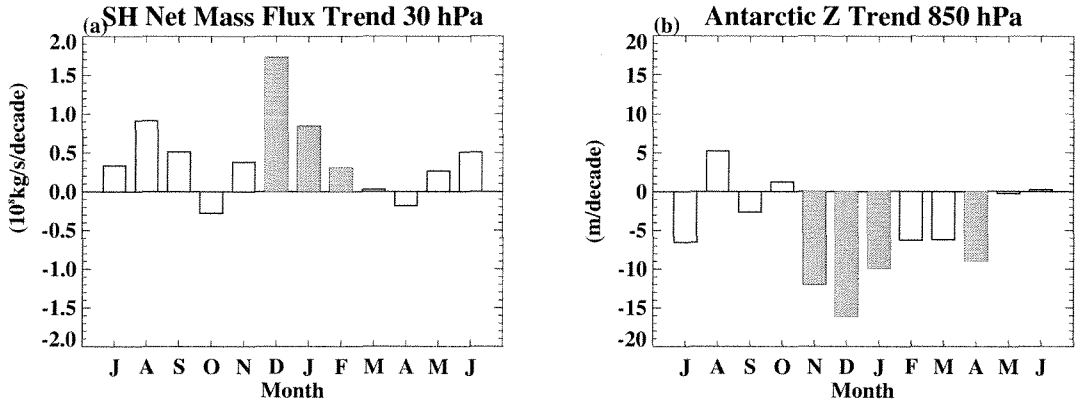

689

690

691 Figure 1: Seasonal cycle of linear trends in the period 1960-2000 for (a) 30 hPa net SH
692 downward mass flux, and (b) 850 hPa Antarctic (65°S-90°S) geopotential height in the
693 P12 simulations. Shading indicates that trends are statistically significant at the 95%
694 confidence level.

695

696

697

697

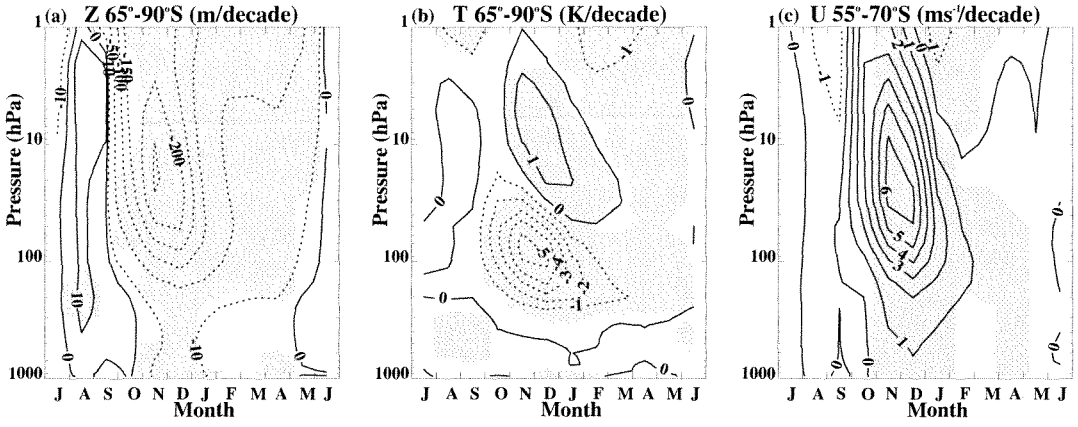

698

699

700 Figure 2: Linear trends plotted as function of month and pressure in (a) Antarctic
701 geopotential height (65°S-90°S), (b) Antarctic temperature (65°S-90°S), and (c)
702 circumpolar zonal wind (55°S-70°S) in the P12 simulations. Shading indicates that trends
703 are statistically significant at the 95% confidence level.

704

705

706

706

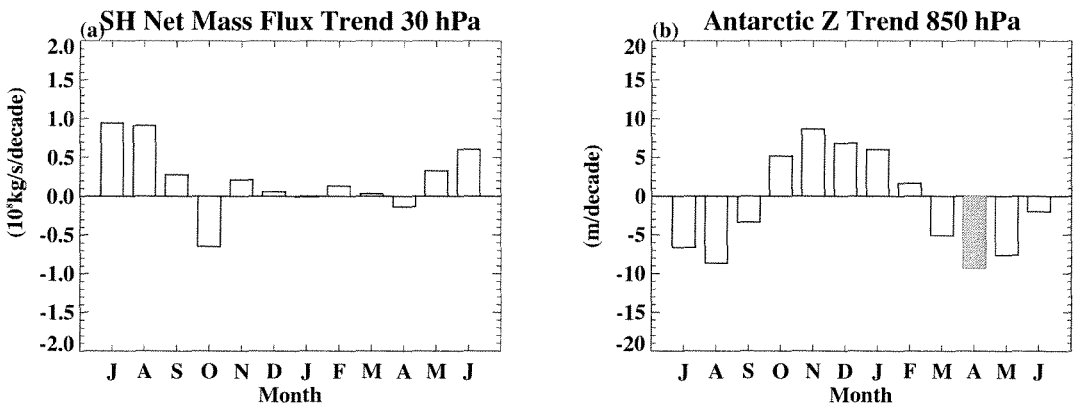

707

708

709 Figure 3: Same as Fig. 1, but for the Cl60 simulation.

710

711

711

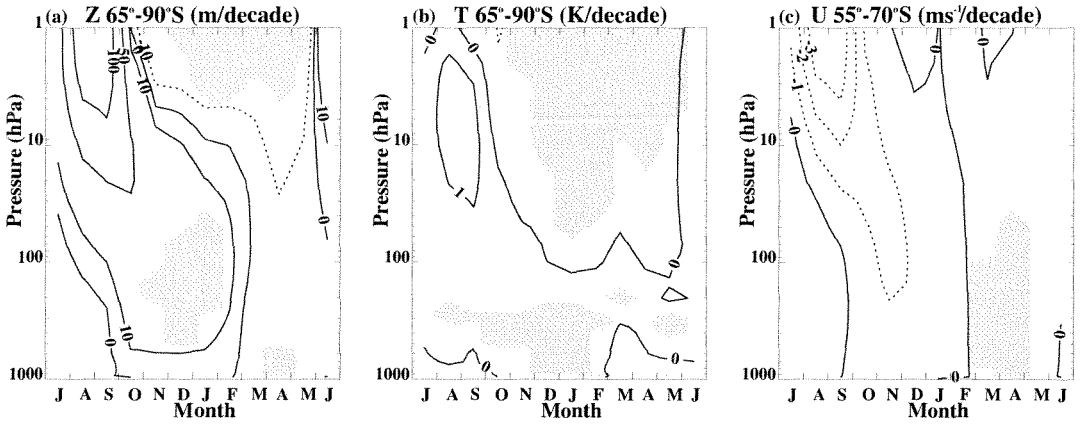

712

713

714 Figure 4: Same as Fig. 2, but for the Cl60 simulation.

715

716

717

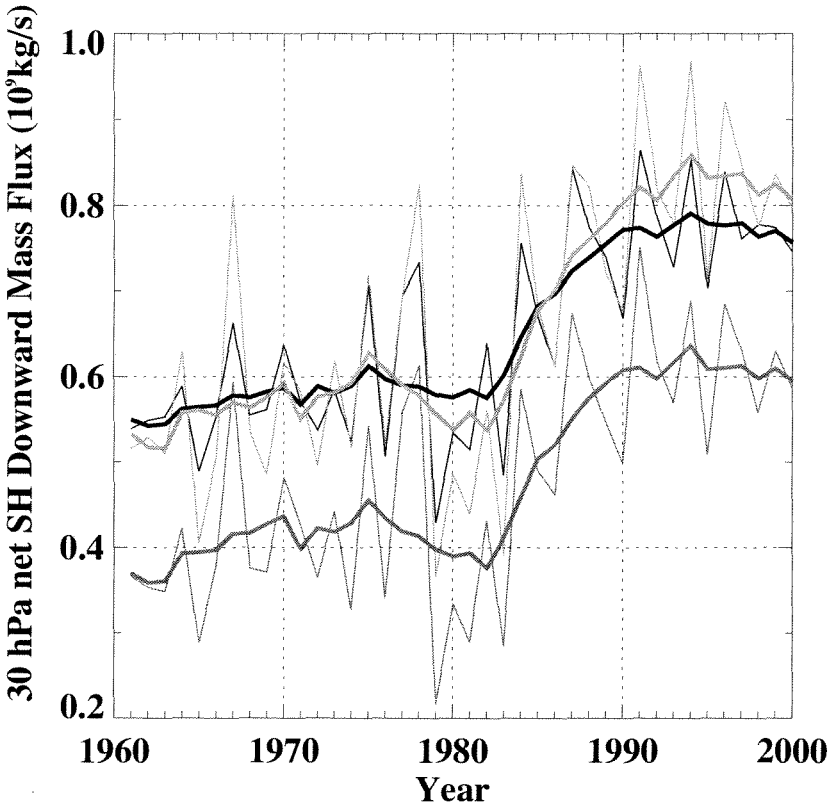

Figure 5: Time series of the NDJF mean net SH downward mass flux at 30 hPa (black). The red and blue lines are the wave-driven mass fluxes calculated from the downward control principle. The red lines show the results from model resolved waves (EP-flux divergence) only. The blue lines show the results including both resolved waves and parameterized gravity waves. The thick curves are 7-year running average mean.

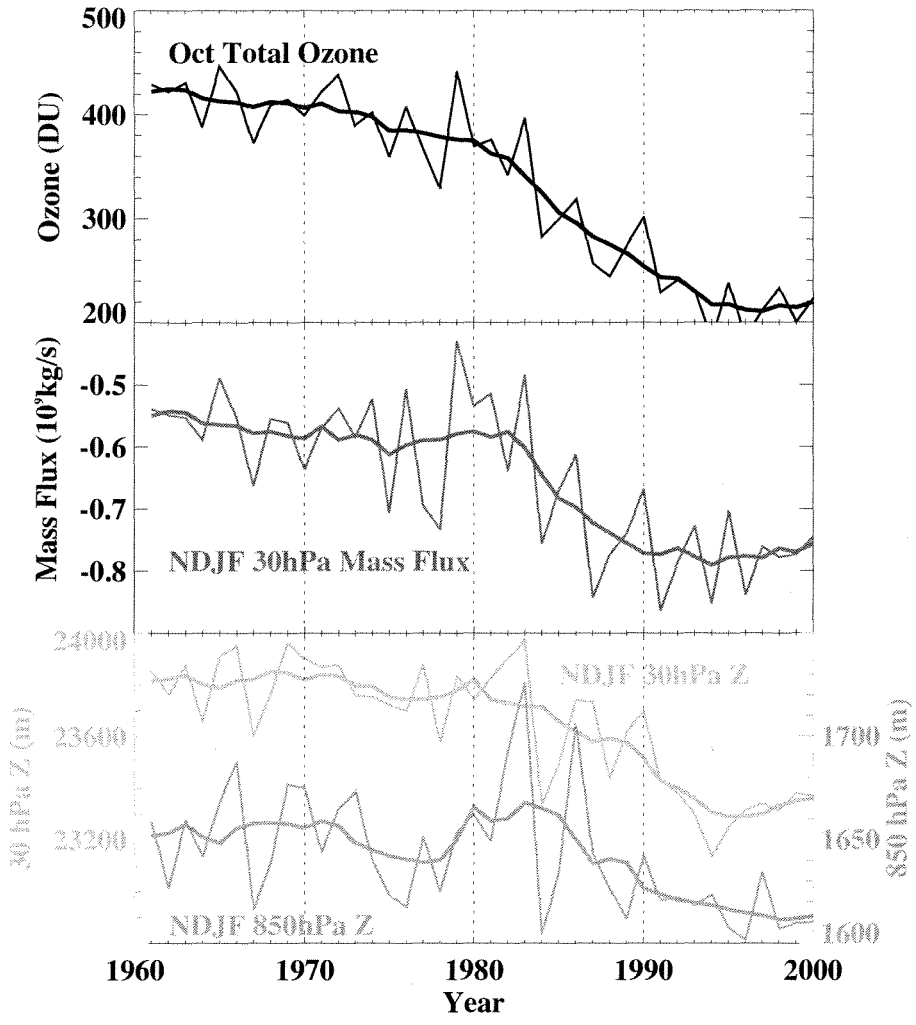

Figure 6: Time series of (upper panel) October Antarctic total ozone; (middle panel) the negative of the NDJF mean net SH mass flux at 30 hPa; and (lower panel) NJDF mean geopotential height at 30 hPa (green, left axis) and 850 hPa (blue, right axis). Thick curves are 7-year running average mean.

734

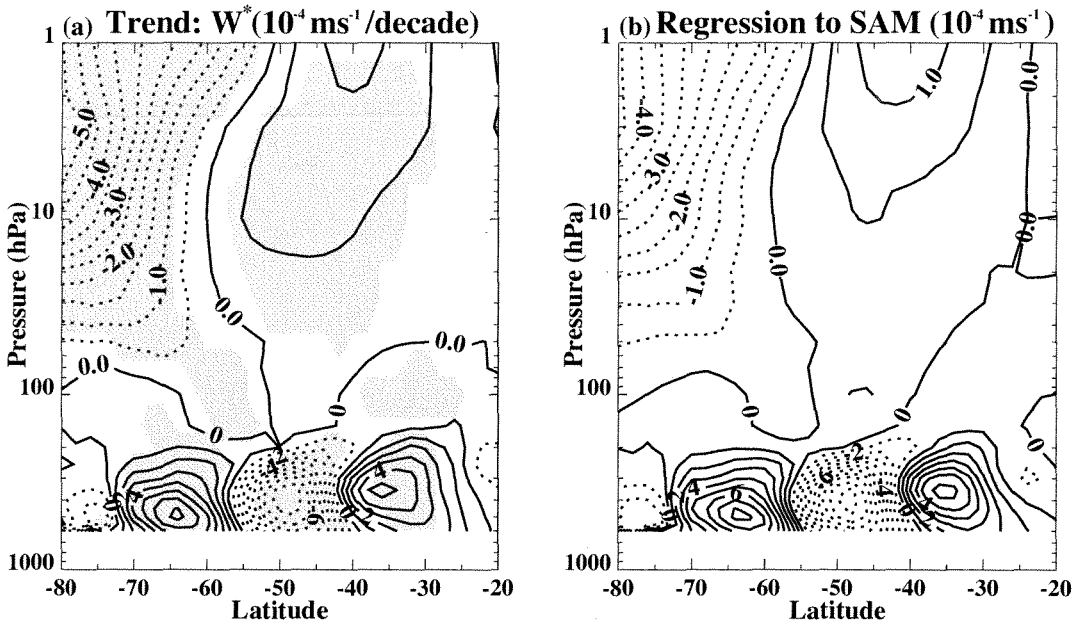

735

736

737 Figure 7: (a) Linear trends of the NDJF residual vertical velocity in the period 1981-2000
738 as a function of latitude and pressure. Shading denotes that trends are significantly
739 different from zero at the 95% confidence level. (b) NDJF residual vertical velocity
740 regressed on the standardized SAM index.

741

742

742

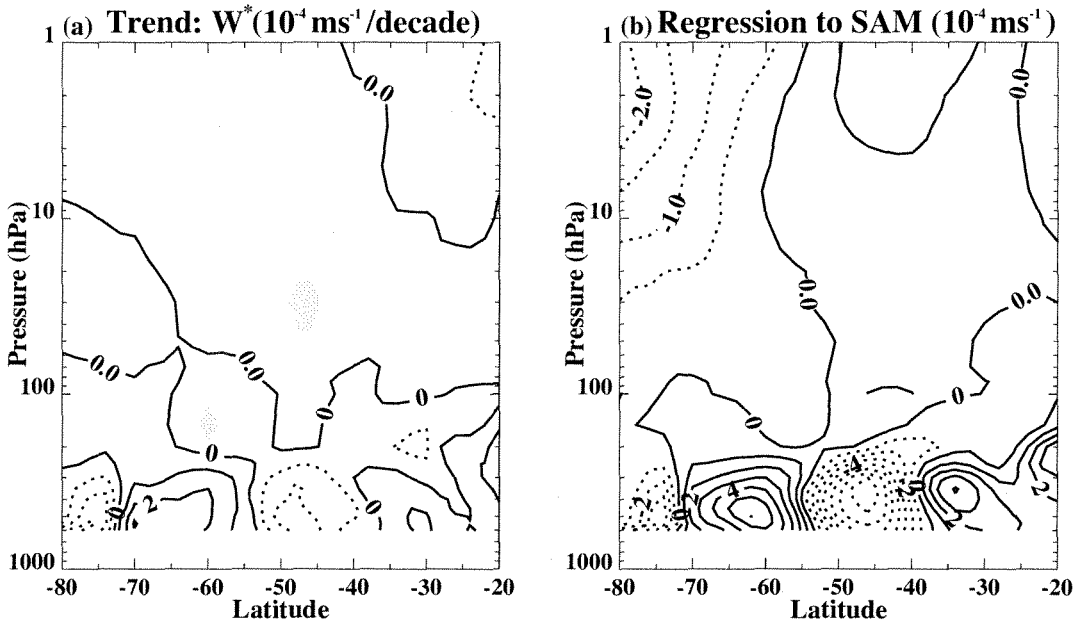

743

744

745 Figure 8: Same as Fig. 7, but for the Cl60 simulation.

746

747

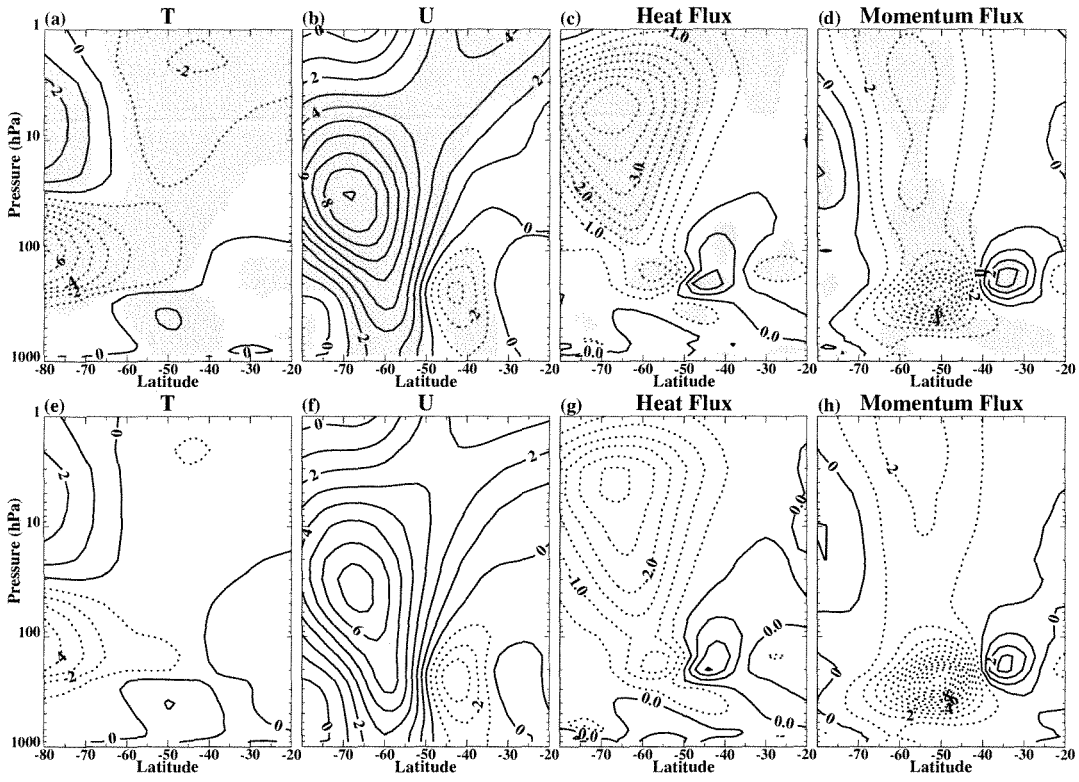

Figure 9: Upper panels show linear trends for the period 1981-2000 as a function of latitude and pressure for the NDJF mean (a) temperature (K/decade), (b) zonal wind (ms^{-1}/decade), (c) northward meridional eddy heat flux (Kms^{-1}/decade), and (d) meridional eddy flux of zonal momentum (m^2s^{-2}/decade) in the P12 simulations. Shading denotes the 95% confidence level. Lower panels are the SAM regression maps for the NDJF mean (e) temperature (K/std SAM), (f) zonal wind (ms^{-1}/std SAM), (g) eddy heat flux (Kms^{-1}/std SAM), and (h) eddy momentum flux (m^2s^{-2}/std SAM).

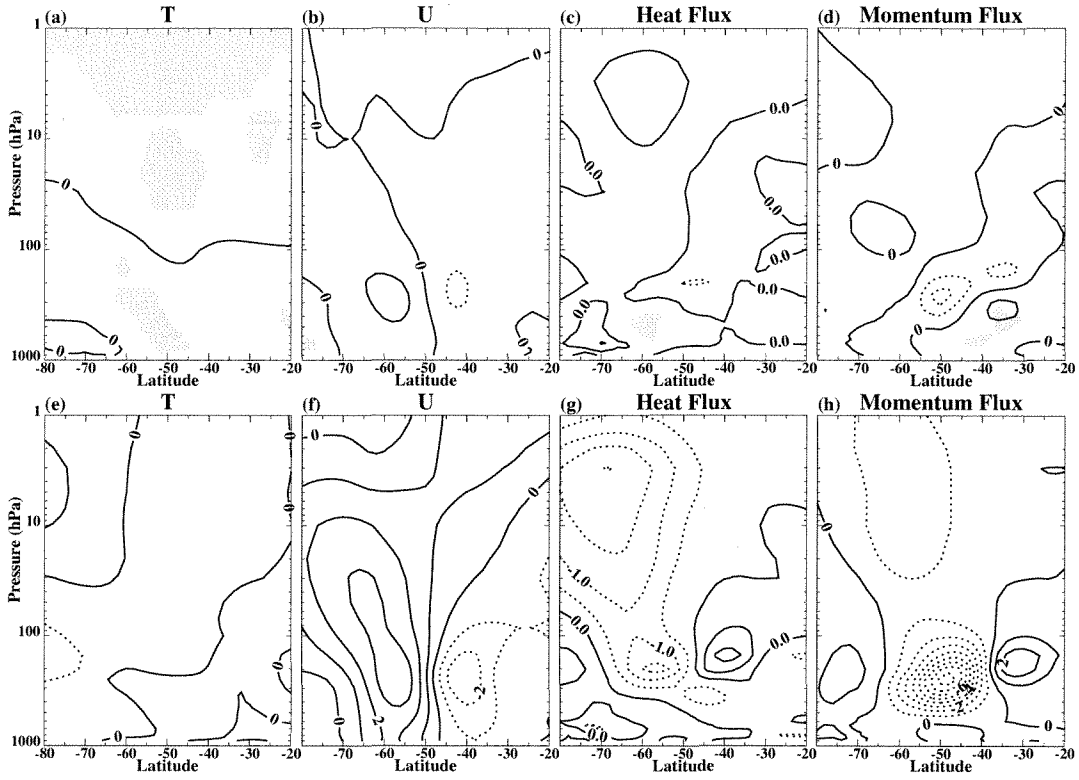

Figure 10: Same as Fig. 9, but for the Cl60 simulation.

763

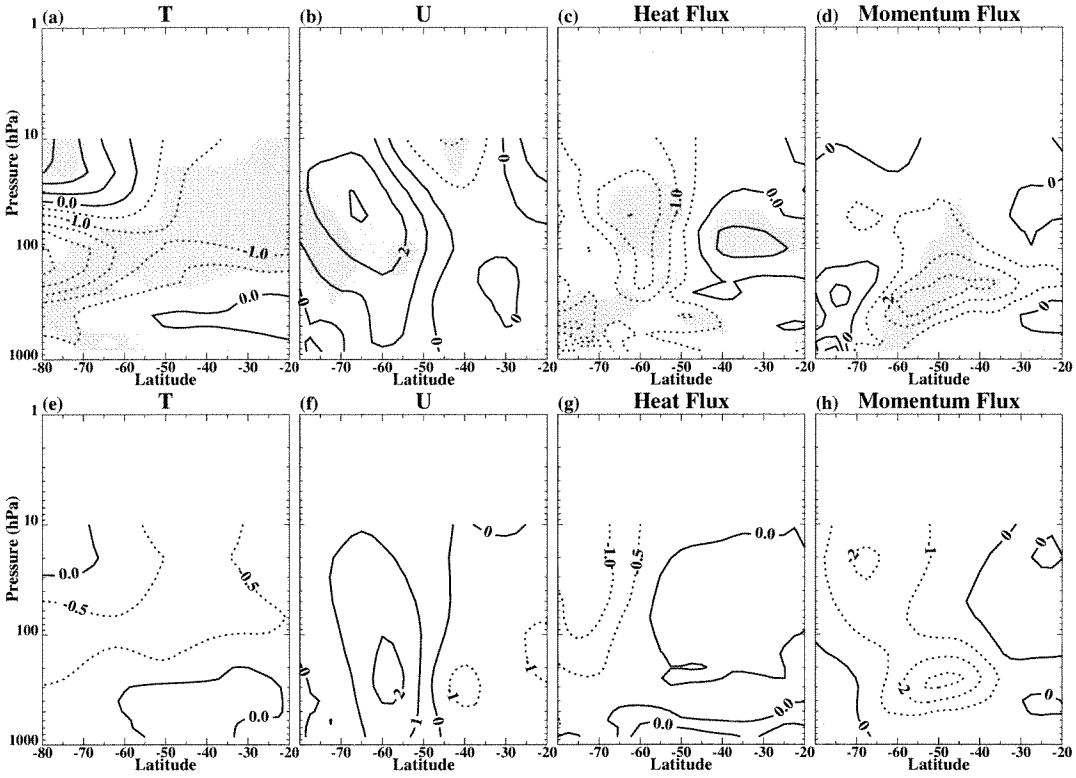

764

765

766 Figure 11: Same as Fig. 9 but calculated from the NCEP Reanalysis 2 data. The dark and
767 light shadings denote 95% and 90% confidence levels, respectively. Note that the NCEP
768 data are only available below 10 hPa.